https://doi.org/10.18321/ectj1565

Properties, Bioactivity and Viability of the New Generation of Oxyfluoronitride Bioglasses

A. Bachar[1,2], A. Mabrouk[3], R. Amrousse[4]*, S. Azat[5], C. Follet[6], C. Mercier[6], F. Bouchart[6]

[1]Laboratoire Génie des Procédés (LGP), Faculté des Sciences, Université Ibnou Zohr, Agadir, Morocco
[2]Faculté des Sciences Appliquées - Ait Melloul, Université Ibnou Zohr Agadir, Morocco
[3]Laboratoire de Recherche en Sciences et Techniques (LRST), Ecole Supérieure de l'Education et de la Formation d'Agadir (ESEFA), Nouveau Complexe Universitaire, Université Ibnou Zohr, Agadir, Morocco
[4]University of Chouaib Doukkali, Faculty of Sciences, 24000 El Jadida, Morocco
[5]Satbayev University, 22a Satbayev str., Almaty, Kazakhstan
[6]Université Polytechnique Hauts-de-France, Laboratoire CERAMATHS/Département Matériaux et Procédés, Maubeuge, France

Article info

Received:
15 October 2023

Received in revised form:
19 December 2023

Accepted:
2 March 2024

Keywords:
Bioactive glass
Oxyfluonitride glass
Mechanical properties
Bioactivity
Cytotoxicity
Biofilm formation

Abstract

In this study, the deposition of apatite on the surface of the glasses with a composition of $22.25Na_2O–13.5CaO–2.5P_2O_5–6.75CaF_2–(55–3x)\ SiO_2–xSi_3N_4$ (x is the no. of moles of Si_3N_4) (where x = 0-4), was studied to examine the influence of nitrogen content on their properties, bioactivity and viability. It was established that density, glass transition temperatures, Young's modulus of elasticity, Vicker's microhardness and fracture toughness increased significantly with increasing nitrogen concentration. Bioactivity was investigated by Fourier Transform Infrared Spectroscopy (FTIR), X-ray Diffraction (XRD), and Hydroxyapatite (HCA) layer thickness was determined using a scanning electron microscope coupled with Energy Dispersive Spectroscopy (SEM-EDS). The bioactivity of the glasses was evaluated by dipping them in a simulated body fluid (SBF) and demonstrated that all glasses are bioactive. Cytotoxicity tests using different concentrations of bioglass powders in a cell growth environment further demonstrated that they were not cytotoxic. The biofilm formation by two bacteria's *E. coli* and *S. marcescens* was characterized by the absorbance of crystal violet. The influence on the presence of bacteria in the form of biofilms appears to be affected by the combination of two main factors: glass reactivity and nitrogen content. Additionally, the type or characteristics of the bacteria also play a significant role in this context.

1. Introduction

Bioglass © is renowned for adhering to living bone in the body through the creation of an apatite coating on its surface [1–3], which expedites the quest for novel bioactive glasses with improved characteristics. The generation of this coating is considered a crucial requirement for bonding with living bone, ensuring successful interaction with the osteoblasts [4–7].

Furthermore, the Hydroxyapatite (HCA) offers a steady and long-lasting connection between the implant and the surrounding setting. As a result, this kind of glass has been created over the recent years in reconstructive surgery to substitute, mend, or enhance sections of the skeletal structure [8–10]. Conversely, the diminished resilience and intrinsic delicacy of Bioglass© have restricted its usage to non-weight-bearing uses [1].

The reduced mechanical potency and intrinsically delicate characteristics of these bioactive glasses have limited their implementation to non-weight-bearing uses [11] such as ossicles in the middle ear and various maxillofacial applications [12, 13]. One

*Corresponding author.
E-mail address: amrousse.r@ucd.ac.ma

approach to enhance the strength of the glasses is by incorporating nitrogen into the silicate framework [14, 15]. It has been demonstrated that as nitrogen substitutes oxygen in silicate glasses, the glass transition temperature, elastic modulus, and hardness rise progressively with the nitrogen proportion [16, 17].

This is because nitrogen offers supplementary interconnection of the glass structure and can thus be viewed as a network-forming anion, considering that the impacts of nitrogen and modifiers on glass characteristics are separate [18]. It has been demonstrated that when nitrogen is introduced into a bioactive Na-Ca-Si glass composition, mechanical attributes are enhanced [19]. Furthermore, it has been indicated that oxynitride glass-ceramics possess promising bioactive qualities [20].

In this study, the Si-Ca-Na-P-O-F-N glasses hold notable significance as they have been proven to be compatible with cell growth in laboratory settings. In these glasses, specific oxygen atoms of the aluminosilicate structure are replaced by nitrogen, resulting in a glass structure comprising [$SiO_{(4-x)}N_x$] tetrahedra (where x = 0-4). The inclusion of nitrogen in the glass structure elevates the thermal and mechanical characteristics, including the glass transition temperature (Tg), microhardness, fracture resistance, and Young's modulus, when compared to oxide glass [20–21].

The introduction of fluorine into calcium SiAlON consistently leads to a decrease in the glass transition temperature (Tg), softening temperature (Tds), refractive index, viscosity, and melting point. However, it has minimal to no impact on density, molar volume, compactness, Young's modulus, or microhardness [21–22].

In this paper, we propose to examine the effects of nitrogen on properties, bioactivity, and viability by incorporating P_2O_5 and CaF_2 into our glass composition. Our team has previously investigated the impact of nitrogen addition in glasses within the quaternary system [16–23]. However, no studies have been found thus far that explore the deposition of apatite on Si-Ca-Na-P-O-F-N glasses, which is the main focus of our current study. The second aim of this research was also to compare the degree of biofilm formation by two bacteria (*E. coli* A324, *Serratia Marcescens*) with increase of the rate of nitrogen. *E. coli* A324 is a non-pathogenic gram-negative strain commonly studied as a model bacterium. It is found in the gastrointestinal tract of mammals, including humans. Certain pathogenic strains, like *E. coli* O157:H7, can cause infections such as Hemolytic Uremic Syndrome (HUS). *Serratia Marcescens* is a gram-negative bacterium that poses a risk to immunocompromised individuals. It is prevalent in hospital settings and associated with nosocomial infections, particularly those related to catheter contamination. *S. marcescens* can cause infections in various body parts and may lead to septicema.

2. Materials and methods

2.1. Preparation of the glasses

On the basis of earlier studies on glass melting and bioactivity carried out by some of the current authors [24], a soda lime base oxide glass containing P_2O_5 has been selected with the following composition (mol%): $22.25Na_2O–13.5CaO–2.5P_2O_5–6.75CaF_2–55SiO_2$. Oxyfluonitride glasses were then prepared with the following molar composition: $22.25Na_2O–13.5CaO–2.5P_2O_5–6.75CaF_2–55SiO_2$ utilizing reagent grade Na_2CO_3 (Merck, purity 99.9%), $CaCO_3$ (Chimie-Plus-Laboratoire, 99%), $(NaPO_3)_n$ (Merck, 99.8% purity), CaF_2 (Carlo Erba, 98%), SiO_2 (Merck, pure quartz) and Si_3N_4 (UBE industries, minimum purity 98%, main impurity: oxygen). The weights of the reagents were determined considering their purity, as given in Table 1.

Table 1. Weight percentages of elements Na-Ca-Si-O-P-F-(N) glasses (T – Theoretical; E – Experimental).

Element	Si		Ca		Na		O		F		P		N	
at %	T	E ±0.3	T	E ±0.2	T ±0.2	E	T ±0.3	E	T ±0.3	E	T ±0.2	E ±0.2	T	E ±0.2
GF0	18.55	19.21	6.82	6.03	15.01	15.21	53.38	54.27	4.55	3.77	1.69	1.51	-	-
GF1	18.68	19.15	6.88	6.01	15.12	16.21	51.69	52.17	4.58	3.7	1.70	1.61	1.35	1.15
GF2	18.80	19.01	6.92	6.24	15.21	15.72	50.01	51.21	4.61	3.82	1.72	1.59	2.73	2.41
GF3	18.93	18.96	6.97	6.87	15.31	15.32	48.30	49.56	4.64	3.91	1.72	1.60	4.13	3.78
GF4	19.06	19.58	7.01	6.93	15.43	16.69	46.54	47.21	4.68	3.76	1.74	1.64	5.54	5.19

The glasses have been developed to maintain constant cationic ratios, regardless of the nitrogen addition. Therefore, the N:O ratio is the single variable of composition that changes and the effects of cation ratio variations on the structure and properties of the glass are eliminating. Early experiments have shown significant weight losses and a solid phosphorus residue formed from the melt. Consequently, as the reaction of P_2O_5 and Si_3N_4 resulted in a loss of P_2 and N_2 [23]. Fluorine forms a complex with calcium and sodium and is present as a mixed calcium and sodium fluoride. The addition of fluorine to the bioglasses lowers the melting temperature, which reduces the loss of nitrogen and the formation of bubbles (Fig. 1). Thus, Fluorine facilitates the dissolution of nitrogen in the melt. The addition of fluorine has enabled us to widen the region of glass formation, making it easier for the modifying cations to dissolve.

The presence of fluorine helped to maintain even greater nitrogen contents in glasses (Table 1), exploiting the well-known beneficial effects of nitrogen incorporation on their physical and mechanical properties.

The basic oxide glasses were initially prepared without P or N, then the nitrogen as of Si_3N_4 was incorporated to the glasses and then the P was added in the next series of steps:

1) Synthesis of base oxide glasses without P_2O_5 with molar proportions: $22.25Na_2O–13.5CaO–2.5P_2O_5–6.75CaF_2–(55–3x)\ SiO_2$. These glasses were melted in air in platinum crucibles at 1350 °C for 30 min.

2) Preparation of $Na_2O–CaO–P_2O_5–CaF_2–SiO_2–Si_3N_4$ glasses by mixing of the crushed base oxide glass powders with varying amounts (x=1, 2, 3, 4) of silicon nitride (Si_3N_4) powder. The powders were weighed and mixed in a glass dish using a magnetic stirrer in 50 ml isopropanol and then the alcohol evaporated by heating. Powder batches were pressed under 300 MPa uniaxial pressure and small powder compacts of 1 cm height were obtained.

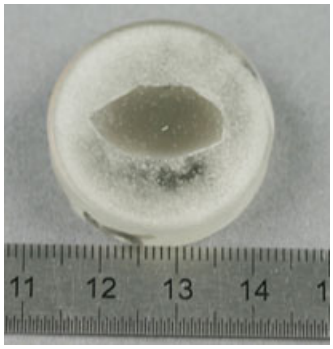

Fig. 1. Typical glass in the Si-Ca-Na-O-P-F-N system.

3) The mixed oxynitride powder compacts were melted in boron nitride lined graphite crucibles in a vertical tube furnace under a flow of high purity N_2 at 1300 °C for 15 min.

4) The resulting crushed oxynitride glass powders were mixed using a magnetic stirrer with the appropriate amount of P_2O_5 in 50 ml of isopropanol, and the alcohol was then evaporated by heating. The powder batches were pressed under a uniaxial pressure of 300 MPa and small powder compacts of 1 cm height were obtained.

5) The final compacts, which contained all components, were melted in boron nitride lined graphite crucibles in a vertical tube furnace under a flow of high purity N_2 at 1300 °C for 15 min.

6) After melting, the glasses were annealed just below the glass transition temperature for 1 h and then slowly cooled to room temperature to eliminate the stresses that would remain after rapid cooling.

2.2. Bioactivity and HCA layer thickness

All cylinders have been embedded in epoxy resin. A glass surface was left unprotected (13 mm diameter disc) and polished with 80 grit paper. The polished glass surfaces were cleaned with acetone and then air-dried. Each sample was immersed in a polystyrene bottle containing 60 mL SBF (simulated body fluid). The ions concentrations and pH of this solution are close to those of human plasma's ones [25–27].

The SBF solution was obtained by dissolving reagent grade chemicals of NaCl, $NaHCO_3$, KCl, $K_2HPO_4.3H_2O$, $MgCl_2.6H_2O$, $CaCl_2.2H_2O$ and Na_2SO_4 in distilled water (Table 2). It was buffered at pH 7.42 with 50 mM tris (hydroxymethyl)-aminomethane and 45 mM HCl. This SBF has been previously confirmed for a variety of bioactive glass type, in order to be capable to reproduce apatite formation on their surfaces as in the living body [28–30]. The samples were kept at 37 ± 0.5 °C for 15 days soaking in SBF.

After the immersion, the samples were washed with deionized water to stop any reaction. The reacted surface films were then studied by Fourier Transform Infrared Spectroscopy (FTIR) in the 1400–400 cm^{-1} wavenumber range and X-ray diffraction. The observations can be affirmed by the Energy Dispersive Spectroscopy (EDS) method.

Table 2. Ion concentrations in SBF and human plasma

pH	Ions Concentration (mM)							
	Na^+	K^+	Mg^+	Ca^{2+}	Cl^-	HCO^{3-}	HPO_4^{2-}	SO_4^{2-}
SBF 7.25-7.42	142.0	5.0	1.5	2.5	147.8	4.2	1.0	0.5
Human plasma 7.24-7.40	142.0	5.0	1.5	2.5	13.0	27.0	1.0	0.5

2.3. Cytotoxicity

Cytotoxicity tests involve viability tests that evaluate the relative efficiency of plating (RPE) and then the lethal concentration at 50% LC50 (or RPE 50) using the colony-forming test on epithelial cell line (L132 cells) [31]. In accordance with international and European standards (ISO10993-5/EN30993-5), the L132 epithelial cell line is selected for its excellent reproducibility and cloning efficiency (approximately 37%) [32]. In a minimum Essential Medium (MEM) supplemented with 10% fœtal calf serum (FCS), L132 cells are continually exposed to progressively increasing concentrations (0, 25, 50 100, 200, 400 mg L^{-1}) of bioglass powder (20 µm diameter granules) with no renewal of the growth environment during the experiments. The positive control is pure nickel powder; mean particle size is 4–6 µm. After a culture period of 9 days, the media is removed and the colonies are stained with a purple crystal. The number of colonies is counted using a binocular microscope. At least six replicate experiments are performed, in triplicate for each concentration group. The results are given as mean values ± SD with respect to the control (an environment without glass powder, 100%). Nickel powder is tested as a positive control for comparison.

2.4. Biofilm formation

The bacterial strains utilized are *Escherichia Coli* and *Serratia Marcescens*, both Gram-negative.

Escherichia coli A324, referred to as *E. coli* A324, is a gram-negative, non-pathogenic strain from the *Enterobacteriaceae* family. *E. coli* is a model bacterium frequently examined by microbiologists. It is a subject of research for comprehending the functioning of bacteria in general. It is commonly present in the gastrointestinal tract of mammals, including humans. Although the strain used is not harmful, certain strains are pathogenic and can cause infections such as *Hemolytic Uremic Syndrome* (*HUS*) (strain O157:H7)[33].

Serratia Marcescens is a gram-negative bacterium from the enterobacteria family, an opportunistic pathogen for humans. This implies that it poses a risk to immunocompromised individuals. Furthermore, it is highly prevalent in hospital settings. *S. marcescens* is associated with nosocomial infections, particularly those linked to catheter contamination. It causes infections in the urinary tract, lacrimal glands, and wounds, and can also lead to septicema [34].

2.4.1. Samples preparation

Biofilm experiments are conducted in groups of three: three consistent samples must be examined to acquire statistically valid outcomes.

Three samples from each glass set *GF0*, *GF1*, *GF2*, *GF3*, *GF4* are positioned in the Luria-Bertani LB medium without any bacteria: these serve as the reference samples. The remaining three samples are exposed to the prepared bacterial solution (LB medium with bacteria): these serve as the experimental samples. Samples are arranged in Petri dishes.

Samples are placed for 48 h, without agitation, at 30 °C, a temperature below the optimum growth temperature for the 2 bacteria (optimum T °C = 37 °C).

In order to quantitatively evaluate the impact of CsrA (*CsrA is a protein that acts as a global regulator in bacteria. It plays a crucial role in controlling the expression of genes involved in various cellular processes, including biofilm formation*) on biofilm

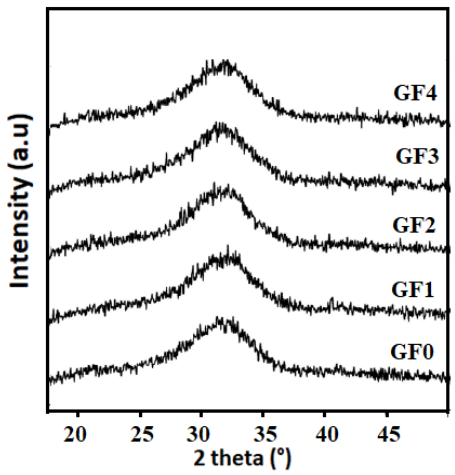

Fig. 2. X-ray diffractograms of the GFx glasses.

Table 3. Properties of Ca-Na-Si-O-P-N-F glasses.

Bioglass	GF0	GF1	GF2	GF3	GF4
N wt.%	0	1.15	2.41	3.78	5.19
Density (g/cm^3)	2.59	2.61	2.64	2.66	2.69
Tg (ºC)	516	528	542	558	574
Tc (ºC)	770	783	797	813	829
HV (GPa)	5.61 ± 0.13	6.01 ± 0.14	6.45 ± 0.13	6.93 ± 0.16	7.42 ± 0.18
E(GPa)indentation method	65.3 ± 2.7	73.9 ± 4.1	83.4 ± 3.6	93.6 ± 5.1	104.2 ± 5.9
Kc(MPa.m$^{1/2}$)	1.13 ± 0.02	1.30 ± 0.03	1.49 ± 0.05	1.69 ± 0.07	1.90 ± 0.06

formation, the growth of biofilms was observed through a crystal violet staining assay, while the growth of planktonic cells in the identical cultures was monitored using absorbance measurements. In the study, biofilm formation is measured using a crystal violet staining assay. This method involves staining the biofilm with crystal violet dye, which binds to the biofilm matrix. The stained biofilm is then quantified by measuring the absorbance of the crystal violet dye. Higher absorbance values indicate a greater amount of biofilm formation. The biofilm formation is indeed measured by crystal violet absorbance in this study. The absorbance measurements provide a quantitative assessment of the amount of crystal violet dye bound to the biofilm, which correlates with the extent of biofilm formation. This method allows for a reliable and reproducible measurement of biofilm formation in the experimental settings.

3. Results and discussion

3.1. Thermal, physical and Mechanical properties of Ca-Na-Si-O-P-N-F glasses

As predicted, all glasses were X-ray amorphous (Fig. 2). The quenched glasses were transparent and macroscopically homogenous, no crystalline phase was observed on the XRD patterns for the glasses.

The determination of density, glass transition temperatures, Young's modulus, micro hardness and Vickers indentation fracture resistance measurements in this work are as described by Bachar et al. [20, 23].

The values of HV (Vickers Hardness) and KIC (Fracture Toughness) obtained by microindentation and E measured by nanoindentation, as well as the density and Tg, Tc values for all the glasses studied are shown in Table 3.

It can be observed that the replacement of oxygen by nitrogen results in significantly linear increases in these properties, but the data do not deviate from the overall tendency. The current results are also consistent with some other data on oxynitride glasses in the literature [14–16].

Density, glass transition temperature and mechanical properties have been shown to increase as nitrogen content increases. This is an indication that the incorporation of nitrogen strengthens the network structure of the glass. This has also been supported in glass systems other than the $CaO–P_2O_5–CaF_2–SiO_2$ system employed in the present study.

The strengthening of the glass network can be justified by considering that the bond between the Si^{4+} and the anion is strengthened by the substitution of the trivalent N^{3-} ion for the divalent O^{2-} ion. The substitution is given in [19, 21].

$$3\,(\text{Si---O---Si}) + 2\,N^{3-} \rightarrow 2\,(\text{Si---}\underset{\substack{|\\ \text{Si}}}{\text{N}}\text{---Si}) + 3\,O^{-2}$$

The extent of crosslinking of the network will increase linearly with eq.% N, resulting in the glass network contracting, increasing the compactness of the glass and decreasing the molar volume in a linear manner.

The changes in properties with the substitution of oxygen by nitrogen, illustrated by the gradients in Table 3, are very much the same as in the Na-Ca-Si-P-O-(N) glass system formerly mentioned [23]. When fluorine replaces oxygen in oxynitride glasses, the maximum nitrogen content can be considerably increased. As a result, the currently calculated gradients are significantly higher than those calculated formerly [23, 39].

3.2. Bioactivity of Ca-Na-Si-P-O-F-(N) System

The most important condition for a biomaterial to bind to living bone is the development an apatite layer in the environment of body fluids on the

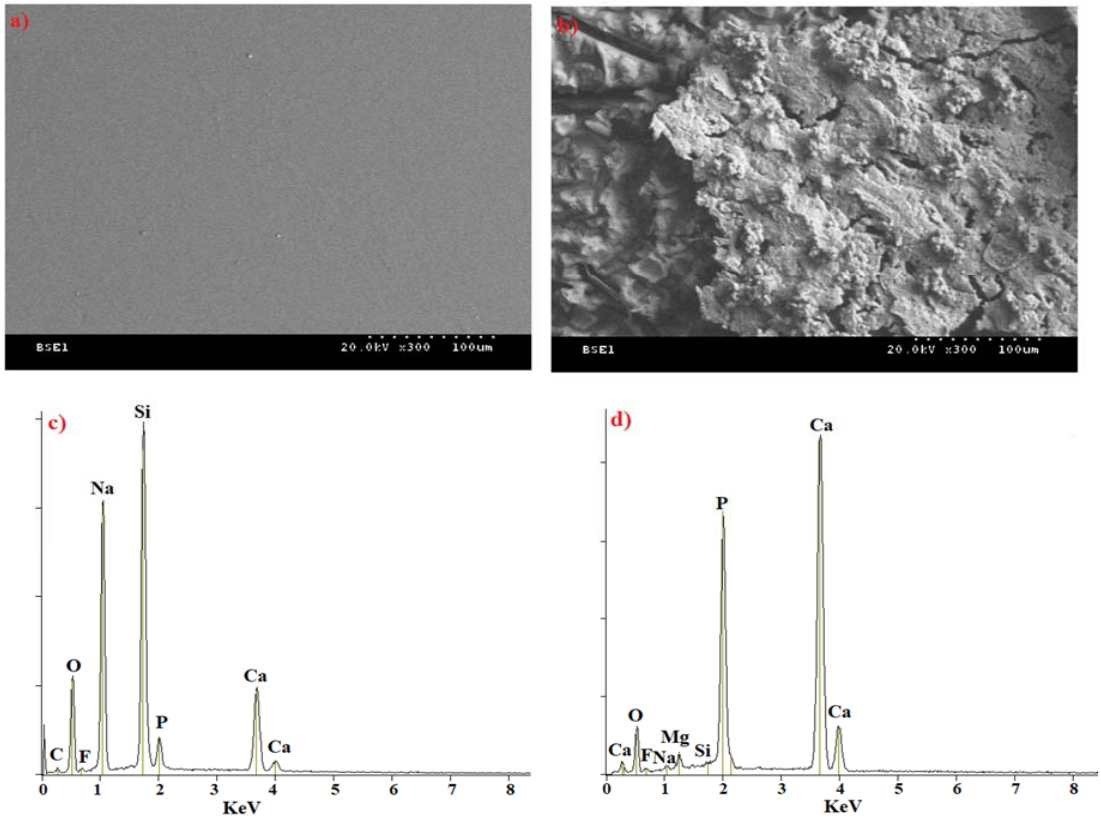

Fig. 3. SEM micrograph of the GF4 glass surface a) before, b) after 15 days soaking in SBF and EDAX analysis of the GF4 glass surface c) before, d) after 15 days soaking in SBF.

surface of the biomaterial. In Fig. 3, scanning electron micrographs (SEM) demonstrate examples of GF4 glass surfaces before and after 15 days in SBF solution. SEM micrographs of the glass surface before immersion in SBF revealed that the structures were empty and free of cracks (Fig. 3a). Nevertheless, after immersion of the glass in SBF, significant cracks and/or voids of 15–35 μm were observed, as shown in Fig. 4b. The EDAX analysis of the GF4 glass before immersion in the SBF shows that the surface presents only the glass constituents (Ca, F, Na, Si and P) as illustrated in Fig. 3c. After immersion in the SBF, the surface was coated with Ca,P (confirmed by EDAX) as indicated in Fig. 3d. The Ca:P ratio of the deposition layer was about 1.6, considering the Ca contribution of the base glass, which is similar to that finding in bone hydroxyapatite (Ca:P = 1.67). The morphology of this Ca,P apatite layer changed from a discrete spherical particle to “coral-like” agglomerates and the amount of apatite deposition diminished slightly as the nitrogen content increased.

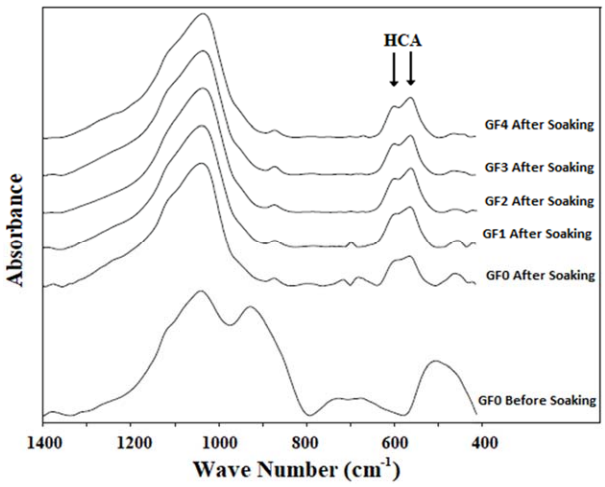

Fig. 4. FTIR spectra of GF0 before soaking and GFx after soaking in SBF.

The evolution of the FTIR spectra of GFx glasses after soaking in the simulated body fluid is presented in Fig. 4. FTIR spectroscopy indicates the appearance of the various layers (silica gel, amorphous calcium phosphate and HCA) as the samples are immersed in SBF. HCA is assumed to begin to crystallize when the 580 cm^{-1} band, assigned to amorphous calcium phosphate, divides into two smaller bands at 610 and 566 cm^{-1}, reflecting the O-P-O bending of hydroxyapatite [33]. The first drawing is made using these crystallization times. The time of HCA formation depends too on the amount of nitrogen. If the amount of nitrogen is too much, the heavily

polymerized network delays the migration of the phosphate groups and slows down the formation of HCA at the surface. Hornez et al. [34] have demonstrated that when nitrogen levels increase in glasses, the network is slower to releasing its CaP groups, resulting in a lower rate of HCA formation. In such a situation, the presence of P_2O_5 allows a significant deposit of CaP on the surface of the material. Under the identical conditions, all GFX bioglasses form HCA on their surface after 15 days of immersion in SBF, thus the presence of phosphorus renders the glasses more bioactive [35].

The presence of phosphorus in the glass promotes the formation of this phase. The quantity of HCA increased with the amount of P_2O_5 in the glass. The high amount of orthophosphate groups within the structure and migrating across the silica-rich layer is the reason for this presence [36]. A higher amount of Na and P enhances the precipitation of CaP from solution and the migration of CaP from the glass across the silica gel layer, resulting in a thick layer of HCA, as shown in Fig. 4. The XRD patterns of the glasses prior to immersion in the SBF solution are identified by an amorphous halo characterizing that all glasses were amorphous (Fig. 2). The XRD patterns got from all GFx samples following immersion in SBF solution for 15 days are illustrated in Fig. 5.

The natural hydroxyapatite pattern is given as a reference (JCPDS Pattern No. 90432) and as a comparison. It demonstrates that a layer of hydroxyapatite is formed on all glass samples, which is confirmed by the three strongest X-ray peaks appearing on 2θ

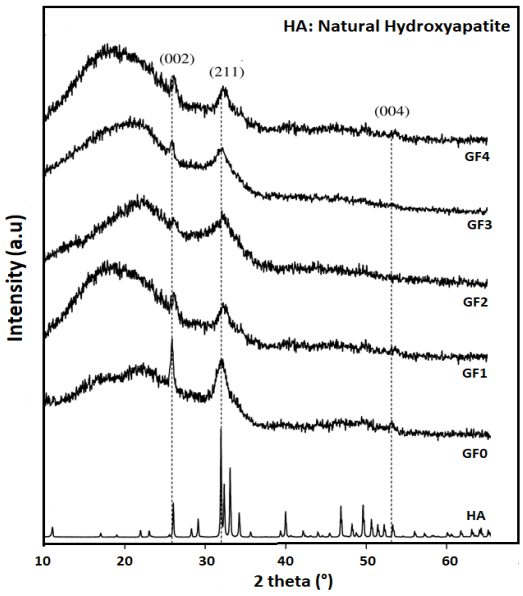

Fig. 5. X-ray diffraction patterns of GFx bioactive glasses after soaking in SBF solution for 15 days.

of 25.50, 31.32 and 51.76 which represent, correspondingly, to the (002), (112) and (004) planes.

A study by Hornez et al. [34] showed that the intensities of the major peaks (002), (211) and (004) decrease with nitrogen content, demonstrating that the crystallinity of this layer constantly decreases with its content, which suggests that nitrogen can prevent bioactivity [34]. In this study, we proved that phosphate favoured the nucleation of hydroxyapatite. Even though GF4 glass contains the high level of nitrogen, we demonstrated that the HA layer formed on the surface of the glass after soaking for 15 days. In the literature [37–38], the adding of low amounts of phosphorus to bioglass compositions (up to 5 mol%) would enhance its reactivity.

In this event, phosphorus has a positive impact on their bioactivity and enhances the rate of appearance of HCA. After 15 days of immersion, the surface of all glasses is totally coated with the HA layer.

3.3. Viability of Ca-Na-Si-P-O-F-(N) System

To demonstrate the non-toxicity of the five samples brought to light, L132 cells were subjected to increasing concentrations of our three glass powders for 9 days. A control measurement devoid of glass powder was also carried out; the number of surviving cells found corresponds to the value of 100%. The control was needed because, regardless of the presence of glass powder, the cells are exposed to stress during their manipulation leading to the death of some of them. When the glass powder is inserted into the medium, the percentage of surviving colonies is only determined from the ratio of the number of colonies remaining with and with no glass.

Figure 6 illustrates the results of the viability tests, carried out on samples of GFx and nickel powder according to the concentration of the powder. Figure 6 shows the non-cytotoxic effect of GFx powders.

Nickel is a compound that will be found to be cytotoxic when added to the culture medium if its addition increases cell death as the compound's concentration increases. In this present case, GFx bioglasses do not exhibit this behavior.

At a concentration of 400 mg L^{-1}, the Mean L132 cell survival is 100% for G1Nx. Therefore, none of the two glasses is cytotoxic. It is important to note that all bioglasses have a survival rate greater than 100% at lower concentrations (103%±4% for GF1 and 107±5% for GF4 with 25 ml.l^{-1}). This result confirms the high cytocompatibility of this sample also at elevated powder concentrations. These glasses provide appropriate substrates to promote cell adhesion and proliferation.

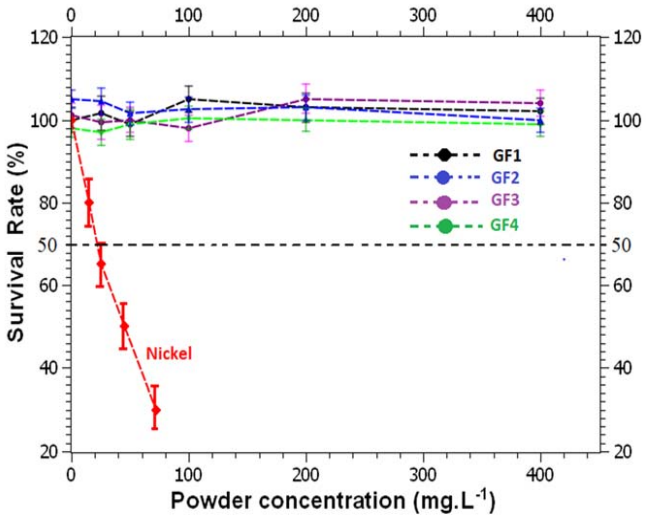

Fig. 6. Viability results for GFx glasses and nickel.

3.4. Estimation of biofilm formation

The relationships between biofilm formation and the absorbance at 570 nm of crystal violet extracted from *E. coli* and *S. marcescens* are illustrated in Fig. 7. In this study, we aimed to assess the effectiveness of crystal violet staining as a method for estimating biofilm formation, particularly in relation to the increasing nitrogen content.

It can be observed that the GFx series glasses exhibit reduced biofilm development with higher nitrogen content for both bacteria. However, *E. coli* shows minimal biofilm formation on GF4 glasses. Conversely, the behavior is different for *S. marcescens.* In conclusion, biofilm formation on material surfaces is influenced by various factors, some of which are yet to be fully explored. For GFx glasses, the presence of bacteria in the form of biofilms appears to be influenced by the combination of two predominant factors: glass reactivity and nitrogen content. Additionally, the nature of the bacteria itself also seems to play a role in biofilm formation. These findings emphasize the complex nature of biofilm formation and highlight the need for further research to better understand the interplay between different factors and optimize strategies for preventing and controlling biofilm-related issues [39]. Crystal violet staining can serve as a valuable tool in assessing biofilm formation and evaluating the efficacy of materials in inhibiting bacterial colonization.

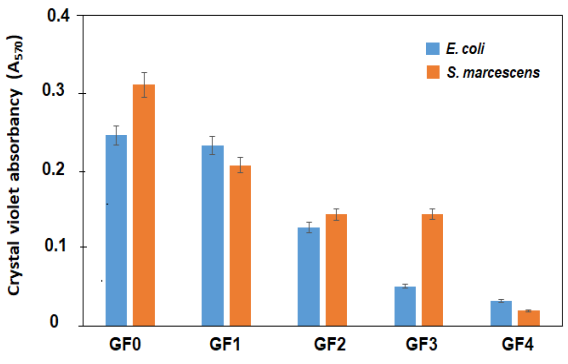

Fig. 7. Evolution of *E. coli* and *S. marcescens* biofilm formation on GFx glasses.

4. Conclusion

To our best understanding, this is the first study on bioactive glasses that contain phosphate, fluorine, and nitrogen. The incorporation of fluoride results in a reduction of Tg, and Tc. The glass transition temperature, hardness, and elastic modulus all increase linearly with the nitrogen rate, suggesting that the incorporation of nitrogen strengthens the glass network because N is in triple coordination with silicon, resulting in additional cross-linking. In this in vitro study, fluoride and phosphate additions act separately to increase apatite formation with both nitrogen-free and nitrogen-containing bioactive glasses [40]. After the glasses were immersed in SBF for 15 days, a homogeneous hydroxyapatite layer formed on the surface of the Na-Ca-Si-P-F-O-N glasses. Moreover, biofilm formation studies have been conducted to assess the performance of these bioactive glasses in preventing bacterial colonization and biofilm formation. Biofilms are complex communities of microorganisms that adhere to surfaces and can cause infections. The findings from these biofilm formation studies are highly promising. The Na-Ca-Si-P-F-O-N glasses exhibit excellent anti-biofilm properties, as evidenced by their ability to resist microbial adhesion and inhibit biofilm formation. The presence of fluoride and phosphate in the glasses contributes to this effect. Furthermore, the homogeneous hydroxyapatite layer formed on the glass surface after immersion in simulated body fluid (SBF) for 15 days acts as a barrier against bacterial colonization, further preventing biofilm formation. In contrast to earlier studies [16–23], the crystallinity of this layer does not decrease with N content, recommending that nitrogen does not prevent bioactivity in the presence of both fluorine and phosphate in glasses. These glasses have been shown to be the most important sites for cell survival, as supported by viability tests demonstrating a cell survival rate of 100±5%. These findings highlight the potential of Na-Ca-Si-P-F-O-N glasses in dental and orthopedic applications [41], where preventing biofilm forma-

tion is crucial for reducing the risk of infections and enhancing patient outcomes. Further research and in vivo studies are needed to validate these results and explore the long-term effectiveness of these glasses in preventing biofilm formation.

References

[1]. M. Cannio, D. Bellucci, J.A. Roether, D.N. Boccaccini, V. Cannillo, *Materials* 14 (2021) 5440. DOI: 10.3390/ma14185440

[2]. S. Hampshire, M.J. Pomeroy, Encyclopedia of glass science, technology, history, and culture. 1st ed. Wiley; (2021) 891–900. DOI: 10.1002/9781118801017.ch7.8

[3]. N.A. Wójcik, B. Jonson, D. Möncke, E.I. Kamitsos, et al., *J. Non Cryst. Solids* 522 (2019) 119585. DOI: 10.1016/j.jnoncrysol.2019.119585

[4]. AR. Garcia, C. Clausell, A. Barba, *Bol. Soc. Esp. Ceram Vidr.* 55 (2016) 209–218. DOI: 10.1016/j.bsecv.2016.09.004

[5]. C. Clausell, A. Barba, J.C. Jarque, A.R. García-Bellés, et al., *J. Am. Ceram. Soc.* 101 (2018) 189–200. DOI: 10.1111/jace.15210

[6]. N.A. Wójcik, B. Jonson, D. Möncke, D. Palles, et al. *J. Non Cryst. Solids* 494 (2018) 66–77. DOI: 10.1016/j.jnoncrysol.2018.04.055

[7]. G.L. Paraschiv, F. Muñoz, G. Tricot, N. Mascaraque, et al., *J. Non Cryst. Solids* 462 (2017) 51–64. DOI: 10.1016/j.jnoncrysol.2017.02.011

[8]. A. Sharafat, B. Forslund, J. Grins, S. Esmaeilzadeh, *J. Mater Sci.* 44 (2009) 664–670. DOI: 10.1007/s10853-008-3058-3

[9]. G.L. Paraschiv, F. Muñoz, L.R. Jensen, Y. Yue, et al., *J. Non Cryst. Solids* 441 (2016) 228. DOI: 10.1016/j.jnoncrysol.2016.03.009

[10]. M.R. Cicconi, A. Veber, D. de Ligny, J. Rocherullé, et al., *J. Lumin.* 183 (2017) 53–61. DOI: 10.1016/j.jlumin.2016.11.019

[11]. C. Park, S. Lee, S. Choi, D. Shin, *Thin Solid Films* 685 (2019) 434–439. DOI: 10.1016/j.tsf.2019.06.055

[12]. J.R. Jones, *Acta Biomater.* 9 (2013) 4457–4486. DOI: 10.1016/j.actbio.2012.08.023

[13]. Y. Su, J. Falgenhauer, A. Polity, T. Leichtweiß, et al., *Solid State Ionics* 282 (2015) 63–69. DOI: 10.1016/j.ssi.2015.09.022

[14]. N. Krishnamacharyulu, G. Jagan Mohini, G. Sahaya Baskaran, V. Ravi Kumar, et al., *J. Alloys Compd.* 734 (2018) 318–328. DOI: 10.1016/j.jallcom.2017.10.271

[15]. S. Ali, A.S. Hakeem, T. Höche, Q.A. Drmosh, et al. (2020) 1–21. Investigation of instinctive defects in nitrogen enrich lanthanum silicon oxynitride glasses. (Research Square is a preprint platform). DOI: 10.21203/rs.3.rs-22643/v1

[16]. S. Hampshire, M.J. Pomeroy, *Appl. Ceram. Tech.* 5 (2008) 155–163. DOI: 10.1111/j.1744-7402.2008.02205.x

[17]. A. Sharafat, B. Jonson, *J. Am. Ceram. Soc.* 94 (2011) 2912–2917. DOI: 10.1111/j.1551-2916.2011.04718.x

[18]. A.R. Hanifi, A. Genson, M.J. Pomeroy, S. Hampshire, *J. Am. Ceram. Soc.* 95 (2012) 600–606. DOI: 10.1111/j.1551-2916.2011.05001.x

[19]. M.J. Pomeroy, E. Nestor, R. Ramesh, S. Hampshire, *Am. Ceram Soc.* 88 (2015) 875–881. DOI: 10.1111/j.1551-2916.2004.00141.x

[20]. A. Bachar, C. Mercier, A. Tricoteaux, A. Leriche, et al., *J. Non Cryst. Solids* 358 (2012) 693–701. DOI: 10.1016/j.jnoncrysol.2011.11.036

[21]. G.L. Paraschiv, S. Gomez, J.C. Mauro, L. Wondraczek, et al., *Phys. Chem. B* 119 (2015) 4109–4115. DOI: 10.1021/jp512235t

[22]. N. Mascaraque, G. Tricot, B. Revel, A. Durán, et. al., *Solid State Ionics* 254 (2014) 40–47. DOI: 10.1016/j.ssi.2013.10.061

[23]. A. Bachar, C. Mercier, C. Follet, N. Bost, et al., *J. Mater. Environ. Sci.* 7 (2016) 347–355. https://www.jmaterenvironsci.com/Document/vol7/vol7_N1/37-JMES-2142-2015-Bachar.pdf

[24]. G.L. Paraschiv, S. Gomez, J.C. Mauro, L. Wondraczek, et al., *J. Phys. Chem. B* 119 (2015) 4109–4115. DOI: 10.1021/jp512235t

[25]. A. Mabrouk, A. Bachar, A. Atbir, C. Follet, et al., *J. Mech. Behav. Biomed. Mater.* 86 (2018) 284–293. DOI: 10.1016/j.jmbbm.2018.06.023

[26]. C. Duée, F. Désanglois, I. Lebecq, C. Follet-Houttemane, *J. Non Cryst. Solids* 358 (2012) 1083–1090. DOI: 10.1016/j.jnoncrysol.2012.02.007

[27]. H. Segawa, N. Hirosaki, S. Ohki, K. Deguchi, et. al. *Opt. Mater.* 42 (2015) 399–405. DOI: 10.1016/j.optmat.2015.01.036

[28]. S. Ahmadi, B. Eftekhari Yekta, H. Sarpoolaky, A. Aghaei, *J. Non Cryst. Solids* 404 (2014) 61–66. DOI: 10.1016/j.jnoncrysol.2014.07.037

[29]. F. Muñoz, R.J. Jiménez-Riobóo, R. Balda, *J. Alloys Compd.* 816 (2020) 152657. DOI: 10.1016/j.jallcom.2019.152657

[30]. G.L. Paraschi, F. Muñoz, L.R. Jensen, R.M. Larsen, et. al., *J. Am. Ceram. Soc.* 101 (2018) 5004–5019. DOI: 10.1111/jace.15747

[31]. A. García-Bellés, C. Clausell, A. Barba, M.J. Pomeroy, et. al., *Ceram Int.* 43 (2017) 4197–4204. DOI: 10.1016/j.ceramint.2016.12.046

[32]. T. Kokubo, H. Takadama, *Biomaterials* 27 (2006) 2907–2915. DOI: 10.1016/J.BIOMATERIALS.2006.01.017

[33]. S.P. Singh, J.F. Schneider, S. Kundu, ACM. Rodrigues, et al., *Mater. Chem. Phys.* 211 (2018) 438–444. DOI: 10.1016/j.matchemphys.2018.02.045

[34]. J.C. Hornez, A. Lefèvre, D. Joly, F. Hildebrand, *Biomol. Eng.* 19 (2002) 103–107. DOI: 10.1016/s1389-0344(02)00017-5

[35]. H.R. Fernandes, A. Gaddam, A. Rebelo, D. Brazete, *Materials* 11 (2018) 2530. DOI: 10.3390/ma11122530

[36]. T. Rouxel, *Philos. Transact. A Math. Phys. Eng. Sci.* 373 (2015). DOI: 10.1098/rsta.2014.0140

[37]. I. Rehman, L.L. Hench, W. Bonfield, R. Smith, *Biomaterials* 15 (1994) 865–870. DOI: 10.1016/0142-9612(94)90044-2

[38]. S. Ali, B. Jonson, M.J. Pomeroy, S. Hampshire, *Ceram. Int.* 41 (2015) 3345–3354. DOI: 10.1016/j.ceramint.2014.11.030

[39]. S. Hampshire, *J. Eur. Ceram. Soc*. 28(2008) 1475–1483. DOI: 10.1016/j.jeurceramsoc.2007.12.021

[40]. M. Vallet-Regi, I. Izquierdo-Barba, A.J. Salinas, *Biomed. Mater. Res.* 46 (1999) 560–565. DOI: 10.1002/(sici)1097-4636(19990915)46:4<560::aid-jbm14>3.0.co;2-m

[41]. F. Muñoz, A. Saitoh, R.J. Jiménez-Riobóo, R. Balda, *J. Non. Cryst. Solids* 473 (2017) 125–131. DOI: 10.1016/j.jnoncrysol.2017.08.005